Characteristic Basis Function Analysis of Large Aperture-Fed Antenna Arrays

Characteristic Basis Function Analysis of Large Aperture-Fed Antenna Arrays

R. Maaskant[1], C. Bencivenni[1], M. V. Ivashina[1],
[1]Signals and Systems Department, Chalmers University of Technology, Gothenburg, Sweden,
rob.maaskant@chalmers.se; carlo.bencivenni@chalmers.se; marianna.ivashina@chalmers.se

***Abstract*—The Characteristic Basis Function Method (CBFM) is applied to rapidly compute the impedance and radiation characteristics of electrically large aperture-fed antenna arrays. A stationary formula for the antenna input admittance matrix is expressed in terms of a product of matrix blocks that are readily available from a method of moment formulation. Numerical results are shown for large arrays of waveguide antennas requiring more than 2 million basis functions, which is reduced by a factor of 9000, so that the solution for the currents are still obtainable in-core on a single desktop computer, while being orders faster than commercial software codes or a standard MoM approach, provided that sufficient memory is available for the Gaussian elimination.**

***Index Terms*—phased array antennas, far-field pattern, method of moments.**

I. Introduction

In this paper, the Characteristic Basis Function Method (CBFM, [1], [2]) is formulated first and then applied to obtain a fast solution of the radiation and impedance characteristics of aperture-fed antenna arrays that are typically being considered as next generation satellite communication antenna systems. Ultimately, the latter involves the design of optimally sparse aperiodic aperture antenna arrays in conjunction with sophisticated beamforming algorithms.

In Sec. II the basic antenna configuration and the voltage excitation sources are described, an electric field integral equation (EFIE) is formulated and discretized using the method of moments, and the input admittance matrix is computed using a stationary formula. The CBFM-enhanced MoM is discussed in Sec. III, which allows to compute the impedance and radiation characteristics of the antenna array in a time-efficient manner. Sec. IV describes the numerical results for a very large aperture antenna array of open-ended waveguide elements.

II. Mathematical Formulation

Consider the aperture-fed array antenna as shown in Fig. 1(a), where only two antenna elements are visualized for simplicity. The antennas are excited by electric field distributions pertaining to the modes in the waveguides feeding the antennas. The apertures are positioned over an infinitely-large perfectly-conducting (PEC) ground plane. The antenna conductors may be lossy.

According to the surface equivalence principle, the electrically thin antenna conductor can be replaced by an equivalent electric current sheet. Also, since we are only interested in the field in the upper half space, we will assume that $\boldsymbol{E} = \boldsymbol{H} = \boldsymbol{0}$ below the ground plane and then fill it with PEC material. On account of the boundary conditions, the aperture electric fields must then be replaced by a compensating source magnetic current placed just above the infinite ground plane. In Figs. 1(b) and (c) we consider the situations 1 and 2, where the equivalent electric surface current $\boldsymbol{J}_1$ arises if $\boldsymbol{M}_1$ is switched on, while $\boldsymbol{M}_2 = \boldsymbol{0}$, whereas $\boldsymbol{J}_2$ arises if $\boldsymbol{M}_2$ is switched on, while $\boldsymbol{M}_1 = \boldsymbol{0}$. Note that the equivalent electric currents $\boldsymbol{J}_{\{1,2\}}$ are supported by the entire conductor surface S, and that the source magnetic currents $\boldsymbol{M}_{\{1,2\}} = \boldsymbol{E}_{\{1,2\}} \times \hat{\boldsymbol{n}}$, where $\hat{\boldsymbol{n}}$ is the unit normal vector as indicated in Fig. 1.

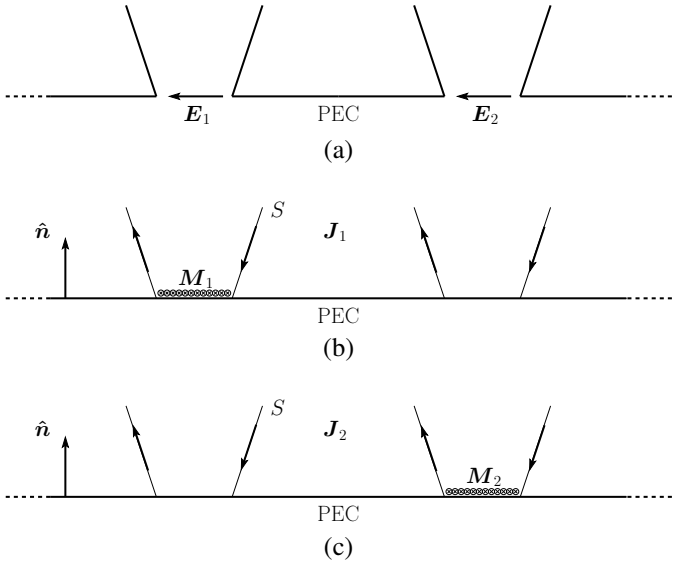

Fig. 1. (a) Original antenna configuration. (b) and (c), equivalent antenna array configurations: in (b) antenna 1 transmits, while other ports are short-circuited; in (c) antenna 2 transmits, while other ports are short-circuited. The original situation is the superposition of the equivalent situations (b) and (c).

One of the objectives is to compute the antenna input admittance matrix. For instance, the mutual admittance Y_{21} between the short-circuited aperture 2, and the source aperture 1, is given by [3, Eq. (42)]

$$Y_{21} = -\frac{1}{V_1 V_2} \iint\limits_{S_2} \boldsymbol{M}_2 \cdot \boldsymbol{H}_1 \, \mathrm{d}S \tag{1}$$

where V_1 and V_2 are the amplitudes of the voltage excitation sources, and S_2 is the surface area of aperture 2. Note that

the total magnetic field is generated by both the electric and magnetic surface currents, i.e., $\boldsymbol{H}_1(\boldsymbol{J}_1, \boldsymbol{M}_1)$.

The radiated fields in Figs 1(b) and (c) can be computed once the source currents $\boldsymbol{J}$ and $\boldsymbol{M}$ are known, i.e., $\boldsymbol{E}(\boldsymbol{J}, \boldsymbol{M})$, and $\boldsymbol{H}(\boldsymbol{J}, \boldsymbol{M})$. The fields from sources and the determination of $\boldsymbol{J}$ through a method-of-moment (MoM) approach is discussed below.

A. The Method of Moment Formulation

To compute the fields from sources in the presence of a PEC ground plane, the image principle is invoked, so that the free-space Green's function can be used for computing the fields from currents and their mirrored counterparts. For the impressed current sources $\boldsymbol{M}$ and $\boldsymbol{J}$, the electric and magnetic fields tangential to the current supporting surfaces can be computed in free space as

$$\boldsymbol{E}_{\text{tan}}(\boldsymbol{J}, \boldsymbol{M}) = \Big[\mathcal{L}(\boldsymbol{J}) - \mathcal{K}(\boldsymbol{M})\Big]_{\text{tan}} - \frac{\hat{\boldsymbol{n}} \times \boldsymbol{M}}{2} \tag{2a}$$

$$\boldsymbol{H}_{\text{tan}}(\boldsymbol{J}, \boldsymbol{M}) = \Big[\mathcal{K}(\boldsymbol{J}) + \frac{1}{\eta_0^2}\mathcal{L}(\boldsymbol{M})\Big]_{\text{tan}} + \frac{\hat{\boldsymbol{n}} \times \boldsymbol{J}}{2} \tag{2b}$$

for $\boldsymbol{r} \in \mathbb{R}^3$, and where η_0 is the free-space wave impedance. Here, the operators are defined as

$$\mathcal{L}(\boldsymbol{X}) = -j\omega\mu_0 \iint_S \boldsymbol{X}(\boldsymbol{r}')G(\boldsymbol{r} - \boldsymbol{r}')\,\mathrm{d}S' + \frac{1}{j\omega\epsilon_0}\boldsymbol{\nabla}\iint_S \boldsymbol{\nabla}' \cdot \boldsymbol{X}(\boldsymbol{r}')G(\boldsymbol{r} - \boldsymbol{r}')\,\mathrm{d}V' \tag{3a}$$

$$\mathcal{K}(\boldsymbol{X}) = \iint_S \boldsymbol{X}(\boldsymbol{r}') \times \boldsymbol{\nabla}' G(\boldsymbol{r} - \boldsymbol{r}')\,\mathrm{d}S' \tag{3b}$$

where $G = \exp(-jk_0R)/(4\pi R)$ is the free-space Green's function, $R = |\boldsymbol{r} - \boldsymbol{r}'|$, and the wavenumber $k_0 = \omega\sqrt{\mu_0\varepsilon_0}$.

In our problem [*cf.* Fig. 1 and Eq. (1)], the electric field $\boldsymbol{E}(\boldsymbol{r})$ will not be observed at the support of the magnetic current $\boldsymbol{M}$. Furthermore, $\boldsymbol{H}(\boldsymbol{r})$ will not be observed at the support of $\boldsymbol{J}$, so that the terms $\hat{\boldsymbol{n}} \times \boldsymbol{M}/2$ and $\hat{\boldsymbol{n}} \times \boldsymbol{J}/2$ in Eq. (2) will not be considered any longer.

To compute an element of the antenna input admittance matrix [see e.g. Y_{21} in Eq. (1)], we first express the magnetic field $\boldsymbol{H}$ as a superposition of the incident and scattered magnetic fields, that is, $\boldsymbol{H} = \boldsymbol{H}^{\text{i}}(\boldsymbol{M}) + \boldsymbol{H}^{\text{s}}(\boldsymbol{J})$. As opposed to $\boldsymbol{M}$, the current $\boldsymbol{J}$ is not known *a priori* but can be found by solving an Electric Field Integral Equation (EFIE) at the antenna conductor surface S. Toward this end, we first impose that the tangential components of the total electric field $\boldsymbol{E} = \boldsymbol{E}^{\text{i}}(\boldsymbol{M}) + \boldsymbol{E}^{\text{s}}(\boldsymbol{J})$ at S must satisfy the Impedance Boundary Condition (IBC)

$$\boldsymbol{E}|_{\text{tan}} = Z_S\boldsymbol{J} \tag{4}$$

where Z_S is the surface sheet impedance. For good conductors of thickness d, one can use that [4]

$$Z_S = \frac{1 - j}{2\sigma\delta\tan((1 - j)d/(2\delta))} \tag{5}$$

where the skin depth $\delta = \sqrt{2/\omega\mu_0\sigma}$. From (2a), we conclude that $\boldsymbol{E}^{\text{i}}_{\text{tan}}(\boldsymbol{M}) = -\mathcal{K}(\boldsymbol{M})|_{\text{tan}}$ and that $\boldsymbol{E}^{\text{s}}_{\text{tan}}(\boldsymbol{J}) = \mathcal{L}(\boldsymbol{J})|_{\text{tan}}$, so that $\boldsymbol{J}$ can be found from (4) by solving the EFIE

$$\mathcal{L}(\boldsymbol{J})|_{\text{tan}} - Z_S\boldsymbol{J} = \mathcal{K}(\boldsymbol{M})|_{\text{tan}}. \tag{6}$$

Next, we expand the electric current $\boldsymbol{J}$ into $N^{[J]}$ vector basis functions $\{\boldsymbol{f}_n^{[J]}\}_{n=1}^{N^{[J]}}$, and the magnetic current $\boldsymbol{M}$ into the set of $N^{[M]}$ vector basis functions $\{\boldsymbol{f}_n^{[M]}\}_{n=1}^{N^{[M]}}$, i.e.,

$$\boldsymbol{J}(\boldsymbol{r}) = \sum_{n=1}^{N^{[J]}} I_n^{[J]}\boldsymbol{f}_n^{[J]}(\boldsymbol{r}), \quad \boldsymbol{M}(\boldsymbol{r}) = \sum_{n=1}^{N^{[M]}} V_n^{[M]}\boldsymbol{f}_n^{[M]}(\boldsymbol{r}) \tag{7}$$

where $\{I_n^{[J]}\}$ and $\{V_n^{[M]}\}$ are the associated set of expansion coefficients. Following Galerkin's moment method, we test the EFIE in (6) $N^{[J]}$ times through the symmetric product $\langle \boldsymbol{a}, \boldsymbol{b}\rangle = \iint \boldsymbol{a} \cdot \boldsymbol{b}\,\mathrm{d}S$ to yield the matrix equation $\mathbf{Z}^{[J,J]}\mathbf{I}^{[J]} = \mathbf{V}^{[J]}$, where the elements of the $N^{[J]} \times N^{[J]}$ complex symmetric matrix $\mathbf{Z}^{[J,J]}$ and the $N^{[J]} \times 1$ excitation vector $\mathbf{V}^{[J]}$ are computed numerically as

$$Z_{mn}^{[J,J]} = \Big\langle \boldsymbol{f}_m^{[J]}, \mathcal{L}(\boldsymbol{f}_n^{[J]}) - Z_S\boldsymbol{f}_n^{[J]} \Big\rangle \tag{8a}$$

$$V_m^{[J]} = -\sum_{n=1}^{N^{[M]}} C_{mn}^{[J,M]}V_n^{[M]} \tag{8b}$$

for $m = 1, 2, \ldots, N^{[J]}$, and where we defined the elements of the $N^{[J]} \times N^{[M]}$ coupling matrix $\mathbf{C}^{[J,M]}$ as $C_{mn}^{[J,M]} = -\langle \boldsymbol{f}_m^{[J]}, \mathcal{K}(\boldsymbol{f}_n^{[M]})\rangle$. For the singular case, i.e. when an observation and source point coincides, special numerical integration routines are used [5]. Note that the elements in the expansion coefficient vector $\mathbf{V}^{[M]}$ are known and fixed as they model the impressed magnetic current associated to a field mode at the port.

B. Antenna Input Admittance Matrix

After solving $\mathbf{I}^{[J]} = \left(\mathbf{Z}^{[J,J]}\right)^{-1}\mathbf{V}^{[J]}$, the antenna input admittance Y_{21} between the ports 2 and 1 [*cf.* Eq. (1)] can be computed. For this purpose, we use that $\boldsymbol{H}_1 = \boldsymbol{H}^{\text{i}}(\boldsymbol{M}_1) + \boldsymbol{H}^{\text{s}}(\boldsymbol{J}_1)$, and Eqs. (1) and (2b), to obtain

$$Y_{21} = -\frac{1}{V_1V_2}\iint_{S_1}\frac{1}{\eta_0^2}\boldsymbol{M}_2 \cdot \mathcal{L}(\boldsymbol{M}_1) + \boldsymbol{M}_2 \cdot \mathcal{K}(\boldsymbol{J}_1)\,\mathrm{d}S. \tag{9}$$

Eq. (9) can be further evaluated by using the expansions in (7), to yield

$$Y_{21} = -\frac{1}{V_1V_2}\left(\sum_{m=1}^{N^{[M]}}\sum_{n=1}^{N^{[M]}}\left[V_{m,2}^{[M]}\frac{1}{\eta_0^2}\Big\langle \boldsymbol{f}_m^{[M]}, \mathcal{L}(\boldsymbol{f}_n^{[M]})\Big\rangle V_{n,1}^{[M]}\right] + \sum_{m=1}^{N^{[M]}}\sum_{n=1}^{N^{[J]}}\left[V_{m,2}^{[M]}\Big\langle \boldsymbol{f}_m^{[M]}, \mathcal{K}(\boldsymbol{f}_n^{[J]})\Big\rangle I_{n,1}^{[J]}\right]\right) \tag{10}$$

which can be compactly written in matrix-vector form, that is,

$$Y_{21} = -\frac{1}{V_1V_2}\left(\mathbf{V}_2^{[M]}\right)^T\left[\mathbf{Y}^{[M,M]}\mathbf{V}_1^{[M]} + \mathbf{C}^{[M,J]}\mathbf{I}_1^{[J]}\right] \tag{11}$$

where we have used that $Y_{mn}^{[M,M]} = \eta_0^{-2}\langle \boldsymbol{f}_m^{[M]}, \mathcal{L}(\boldsymbol{f}_n^{[M]})\rangle$, and that $C_{mn}^{[M,J]} = \langle \boldsymbol{f}_m^{[M]}, \mathcal{K}(\boldsymbol{f}_n^{[J]})\rangle$, so that $\mathbf{C}^{[M,J]} = -\left(\mathbf{C}^{[J,M]}\right)^T$, since testing $\boldsymbol{H}(\boldsymbol{J})$ with $\boldsymbol{M}$ is a minus sign different from testing $\boldsymbol{E}(\boldsymbol{M})$ with $\boldsymbol{J}$ [see Eq. (2)]. Furthermore, $\mathbf{I}^{[J]} = \left(\mathbf{Z}^{[J,J]}\right)^{-1}\mathbf{V}^{[J]}$, and $\mathbf{V}^{[J]} = -\mathbf{C}^{[J,M]}\mathbf{V}^{[M]}$ [see Eq. (8b)]. Hence, (11) can also be written as

$$Y_{21} = -\frac{1}{V_1 V_2}\left(\mathbf{V}_2^{[M]}\right)^T \Big[\mathbf{Y}^{[M,M]} - \mathbf{C}^{[M,J]}\left(\mathbf{Z}^{[J,J]}\right)^{-1}\mathbf{C}^{[J,M]}\Big]\mathbf{V}_1^{[M]} \quad (12)$$

Eq. (12) consists of two contributions: (i) $\boldsymbol{H}^{\mathrm{i}}(\boldsymbol{M}_1)$ that is generated by the source magnetic current $\boldsymbol{M}_1$ which is tested by the source magnetic current $\boldsymbol{M}_2$, and; (ii) $\boldsymbol{H}^{\mathrm{s}}(\boldsymbol{J}_1(\boldsymbol{M}_1))$ that is generated by the same source magnetic current $\boldsymbol{M}_1$ which, in turn, induces an electrical current $\boldsymbol{J}_1$ that gives rise to a scattered magnetic field $\boldsymbol{H}^{\mathrm{s}}(\boldsymbol{J}_1)$ which is also tested by $\boldsymbol{M}_2$.

C. Antenna Radiation Pattern

The normalized far-field functions $\{\boldsymbol{E}_{\text{far}}, \boldsymbol{H}_{\text{far}}\}$, observed at the surface of a sphere, for $R \to \infty$, can be computed with the aid of (2), i.e.,

$$\boldsymbol{E}_{\text{far}}(\theta,\phi) = \mathcal{L}_\infty(\boldsymbol{J}) - \mathcal{K}_\infty(\boldsymbol{M}) \quad (13a)$$

$$\boldsymbol{H}_{\text{far}}(\theta,\phi) = \hat{\boldsymbol{r}} \times \boldsymbol{E}_{\text{far}}/\eta_0 \quad (13b)$$

where we have defined the far-field operators $\mathcal{L}_\infty$ and $\mathcal{K}_\infty$, for observation points on the far-field sphere, as

$$\mathcal{L}_\infty(\boldsymbol{X})(\theta,\phi) = Re^{jkR}\mathcal{L}(\boldsymbol{X})(\boldsymbol{r}), \quad R \to \infty \quad (14a)$$

$$\mathcal{K}_\infty(\boldsymbol{X})(\theta,\phi) = Re^{jkR}\mathcal{K}(\boldsymbol{X})(\boldsymbol{r}), \quad R \to \infty. \quad (14b)$$

In terms of the basis functions, i.e. by using Eq. (7),

$$\boldsymbol{E}_{\text{far}} = \sum_{n=1}^{N^{[J]}} I_n^{[J]}\mathcal{L}_\infty(\boldsymbol{f}_n^{[J]}) - \sum_{n=1}^{N^{[M]}} V_n^{[M]}\mathcal{K}_\infty(\boldsymbol{f}_n^{[M]}) \quad (15)$$

$$= \sum_{n=1}^{N^{[J]}} I_n^{[J]}\boldsymbol{g}_n^{[J]} - \sum_{n=1}^{N^{[M]}} V_n^{[M]}\boldsymbol{g}_n^{[M]} \quad (16)$$

where the electric far-field functions of the basis function currents $\boldsymbol{g}_n^{[J]}(\theta,\phi) = \mathcal{L}_\infty(\boldsymbol{f}_n^{[J]})$ and $\boldsymbol{g}_n^{[M]}(\theta,\phi) = \mathcal{K}_\infty(\boldsymbol{f}_n^{[M]})$. Note that, with the above definitions, the time-average total radiated power P_{rad} is defined as $P_{\text{rad}} = 1/2\,\Re\mathfrak{e}\iint_{S_\infty}\boldsymbol{E}_{\text{far}} \times \boldsymbol{H}_{\text{far}}^*\,\mathrm{d}\Omega$, where the solid angle $\mathrm{d}\Omega = \sin(\theta)\,\mathrm{d}\theta\,\mathrm{d}\phi$.

III. The Characteristic Basis Function Method

In this paper, the CBFM is applied to reduce the size of the moment matrix equation $\mathbf{Z}^{[J,J]}\mathbf{I}^{[J]} = \mathbf{V}^{[J]}$ [*cf.* also Eq. (8a)]. Following the CBFM for antenna array problems [6], the array of N_{el} antenna elements is subdivided into N_{el} subdomains to contain one antenna element per subdomain. We employ the $K_p^{[J]}$ Characteristic Basis Functions (CBFs) $\{\boldsymbol{J}_{p,s}^{\text{CBF}}\}_{s=1}^{K_p^{[J]}}$ for the electric current on the pth subdomain, where $p = 1, 2, \ldots, N_{\text{el}}$. The sth CBF $\boldsymbol{J}_{p,s}^{\text{CBF}}$ on the pth subdomain is, in turn, expanded into the $N_p^{[J]}$ lower-level basis functions $\{\boldsymbol{f}_{n,p}^{[J]}\}_{n=1}^{N_p^{[J]}}$ for the electric current on the pth subdomain with fixed expansion coefficients $\{I_{n,p,s}\}$, i.e.,

$$\boldsymbol{J}_{p,s}^{\text{CBF}} = \sum_{n=1}^{N_p^{[J]}} I_{n,p,s}\boldsymbol{f}_{n,p}^{[J]} \quad (17)$$

Hence, the total electric current $\boldsymbol{J}$ is expanded as

$$\boldsymbol{J} = \sum_{p=1}^{N_{\text{el}}}\sum_{s=1}^{K_p^{[J]}} I_{p,s}^{\text{CBF}}\boldsymbol{J}_{p,s}^{\text{CBF}} = \sum_{n=1}^{N_{\text{CBF}}^{[J]}} I_n^{\text{CBF}}\boldsymbol{J}_n^{\text{CBF}} \quad (18)$$

where $\{I_{p,s}^{\text{CBF}}\}$, or $\{I_n^{\text{CBF}}\}$, are the $N_{\text{CBF}}^{[J]}$ unknown expansion coefficients for the CBFs associated to the electric current. It can be shown that, when employing (18) to discretize the EFIE in (6), the following reduced moment matrix equation is obtained:

$$\begin{bmatrix} \mathbf{I}_1^T\mathbf{Z}_{11}^{[J,J]}\mathbf{I}_1 & \cdots & \mathbf{I}_1^T\mathbf{Z}_{1,N_{\text{el}}}^{[J,J]}\mathbf{I}_{N_{\text{el}}} \\ \vdots & \ddots & \vdots \\ \mathbf{I}_{N_{\text{el}}}^T\mathbf{Z}_{N_{\text{el}},1}^{[J,J]}\mathbf{I}_1 & \cdots & \mathbf{I}_{N_{\text{el}}}^T\mathbf{Z}_{N_{\text{el}},N_{\text{el}}}^{[J,J]}\mathbf{I}_{N_{\text{el}}} \end{bmatrix} \begin{bmatrix} I_1^{\text{CBF}} \\ \vdots \\ I_{N_{\text{CBF}}^{[J]}}^{\text{CBF}} \end{bmatrix} = \begin{bmatrix} \mathbf{I}_1^T\mathbf{V}_1^{[J]} \\ \vdots \\ \mathbf{I}_{N_{\text{el}}}^T\mathbf{V}_{N_{\text{el}}}^{[J]} \end{bmatrix} \quad (19)$$

where $\mathbf{Z}_{pq}^{[J,J]}$ is the moment matrix block pertaining to the lower-order basis functions on the observation subdomain p and source subdomain q, and $\mathbf{V}_p^{[J]}$ is the excitation coefficient vector for the $N_p^{[J]}$ lower-order basis functions $\{\boldsymbol{f}_{n,p}^{[J]}\}$ on the pth subdomain for the electric current. The matrix $\mathbf{I}_p$ is of size $N_p^{[J]} \times K_p^{[J]}$, where the sth column of $\mathbf{I}_p$ represents the sth CBF for the electric current on the pth subdomain in accordance with (17). The reduced moment matrix $\mathbf{Z}_{\text{red}}^{[J,J]}$ in the reduced matrix equation $\mathbf{Z}_{\text{red}}^{[J,J]}\mathbf{I}^{\text{CBF}} = \mathbf{V}_{\text{red}}^{[J]}$ in (19) is of size $N_{\text{CBF}}^{[J]} \times N_{\text{CBF}}^{[J]}$.

As opposed to $\mathbf{I}^{\text{CBF}}$, the expansion coefficients in (17) are predetermined and then fixed to prescribe each CBF. To generate these fixed expansion coefficient vectors, we solve for several currents on a single antenna element in a smaller subarray, for example by exciting the subarray elements one-by-one. The so-induced currents on the pth subdomain are then used as CBFs, whose expansion coefficient vectors form the columns of $\mathbf{I}_p$. A detailed description on the herein applied CBF generation procedure can be found in [7], where the problem of electrically interconnected subdomains and partially overlapping CBFs is discussed in [8]. It is pointed out that the number of basis functions is reduced through the application of the Singular Value Decomposition (SVD) with an appropriate thresholding procedure on the singular values [9], and that the Adaptive Cross Approximation (ACA) algorithm is invoked to rapidly construct $\mathbf{Z}_{\text{red}}^{[J,J]}$ [7].

Once the matrix equation $\mathbf{Z}_{\text{red}}^{[J,J]}\mathbf{I}^{\text{CBF}} = \mathbf{V}_{\text{red}}^{[J]}$ in (19) has been solved, the current $\boldsymbol{J} = \sum_{n=1}^{N_{\text{CBF}}^{[J]}} I_n^{\text{CBF}}\boldsymbol{J}_n^{\text{CBF}}$ can be computed. One can also expand the magnetic current in term of CBFs, $\boldsymbol{M} = \sum_{n=1}^{N_{\text{CBF}}^{[M]}} V_n^{\text{CBF}}\boldsymbol{M}_n^{\text{CBF}}$ to model each waveguide mode. Analogously to the derivation for (12), when employing CBFs for the electric and magnetic currents, it can be shown that the

mutual admittance Y_{21}^{pq} between the qth waveguide mode at port 1 and the pth waveguide mode at port 2 is computed as

$$Y_{21}^{pq} = -\frac{1}{V_1^q V_2^p}\left(\mathbf{V}_2^{\mathrm{CBF},p}\right)^T \left[\mathbf{Y}_{\mathrm{red}}^{[M,M]} - \mathbf{C}_{\mathrm{red}}^{[M,J]}\left(\mathbf{Z}_{\mathrm{red}}^{[J,J]}\right)^{-1}\mathbf{C}_{\mathrm{red}}^{[J,M]}\right]\mathbf{V}_1^{\mathrm{CBF},q} \quad (20)$$

where $\mathbf{Z}_{\mathrm{red}}^{[J,J]}$, $\mathbf{Y}_{\mathrm{red}}^{[M,M]}$, $\mathbf{C}_{\mathrm{red}}^{[M,J]}$, and $\mathbf{C}_{\mathrm{red}}^{[J,M]}$ are the reduced matrices instead, along with the CBF expansion coefficient vectors $\mathbf{V}_1^{\mathrm{CBF},p}$ and $\mathbf{V}_1^{\mathrm{CBF},q}$ for the corresponding magnetic currents (i.e. waveguide modes) and ports. The corresponding mode excitation voltages are V_1^p and V_1^q.

Finally, the far-field function $\boldsymbol{E}_{\mathrm{far}}$ in (15) can be expressed in terms of the CBF patterns $\boldsymbol{g}_n^{\mathrm{CBF},[J]}$ and $\boldsymbol{g}_n^{\mathrm{CBF},[M]}$, i.e.,

$$\boldsymbol{E}_{\mathrm{far}} = \sum_{n=1}^{N_{\mathrm{CBF}}^{[J]}} I_n^{\mathrm{CBF}}\boldsymbol{g}_n^{\mathrm{CBF},[J]} - \sum_{n=1}^{N_{\mathrm{CBF}}^{[M]}} V_n^{\mathrm{CBF}}\boldsymbol{g}_n^{\mathrm{CBF},[M]}. \quad (21)$$

Note that, for array antennas with identical antenna elements, some of the subdomains support identical sets of CBFs, so that the corresponding sets of CBF-patterns differ only by the phase factor $\exp(jk_o\boldsymbol{r}_{pq}\cdot\hat{\boldsymbol{r}}(\theta,\phi))$, where $\boldsymbol{r}_{pq}$ is the relative offset vector between the subdomains p and q, and $\hat{\boldsymbol{r}} = \sin(\theta)\cos(\phi)\hat{\boldsymbol{x}} + \sin(\theta)\sin(\phi)\hat{\boldsymbol{y}} + \cos(\theta)\hat{\boldsymbol{z}}$.

IV. Numerical Results

The CBFM computations have been carried out on a 64 bit (x86-64) Linux – openSUSE (v.12.3) server equipped with 2 Intel Xeon E5640 CPUs operating at 2.67 GHz (each CPU has 4 cores/8 threads), with access to 144 GB RAM memory and 2 TB harddisk space.

For the numerical computations, an open-ended corrugated circular waveguide antenna element as classified by RUAG Space (Sweden) has been used as depicted in Fig. 2(a). The element is excited by the fundamental TE_{11} mode. The resulting E- and H-plane gain patterns (@18.3 GHz) are shown in Fig. 2(b) and are in good agreement with the simulation results obtained by the FEKO software (less than 1% rel. error).

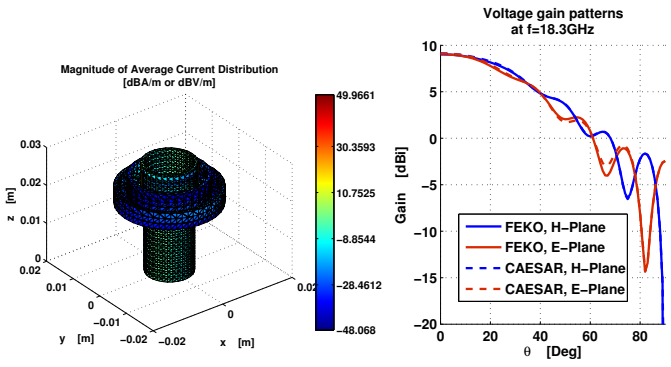

(a) (b)

Fig. 2. (a) Magnitude of current distribution (@18.3 GHz) of a TE_{11}-mode excited open-ended corrugated circular waveguide. (b) Comparison of E- and H-plane gain patterns with the FEKO simulation software.

Next, an identically meshed waveguide antenna element is applied in a large array of 317 elements, each employing 9030 Rao-Wilton-Glisson basis functions for the electric current, and 189 RWGs for the waveport magnetic current, i.e., in total 2,922,423 RWGs. The diameter of the array at 18.3 GHz is $\sim 45\lambda$. Primary and secondary CBFs are generated as explained

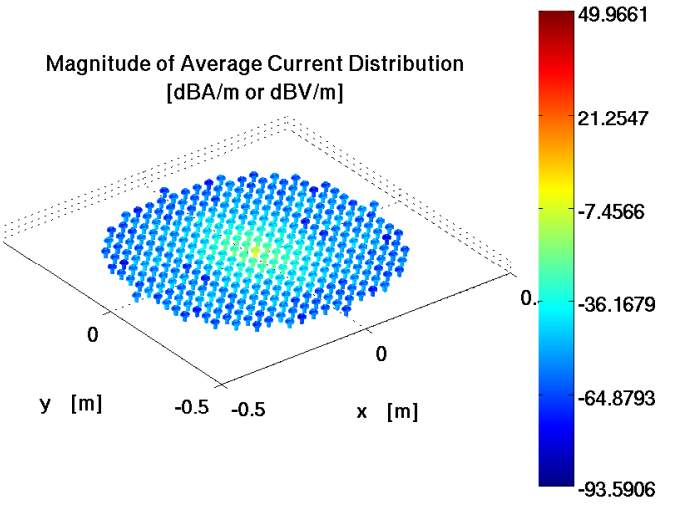

Fig. 3. Magnitude of current distribution (@18.3 GHz) of a 317 Element array of open-ended corrugated circular waveguides. Center element excited, surrounding elements short-circuited.

in [1] for a radius of 4λ, however, along with a typical SVD threshold of 10^{-2}, only a single CBF is retained per element out of the 9 that were initially generated. Hence, only 317 CBFs are employed for the entire array. This huge compression ($\sim$ factor 9000) can be attributed to the relatively low mutual coupling between the array elements, which is typically less than 15 dB, so that the employment of a single mode current per antenna element suffices. However, mutual coupling effects between the single mode currents is still of importance for the accurate modeling of the far sidelobes.

The time for generating CBFs is 4 min. 33 sec., for building the reduced matrix 2h. 2min. and 44 sec., and the solution of the (317$\times$ 317) reduced matrix equation is performed in split seconds. The total simulation time is 140 min. and 35 sec., which includes also the construction of the reduced excitation vector.

V. Conclusions and Recommendations

The CBFM has both been formulated and implemented for analyzing large aperture-fed antenna arrays. The numerical accuracy of the proposed algorithm has been assessed by the FEKO software through a singly-excited TE_{11} open-ended corrugated circular waveguide antenna, and an example of a 317 element array of these elements has been analyzed on a dual-CPU computer system. The original problem requires us to employ over 2 million basis functions, but this amount can be reduced to only 317 macro basis functions because

of the relatively weak mutual coupling between antenna array elements. However, coupling effects should not be ignored for the accurate modeling of far side lobes.

ACKNOWLEDGMENT

This work is a collaborative effort between Chalmers, RUAG Space, Ericsson and KTH, funded by the Swedish Agency for Innovation System VINNOVA and the CHASE centre, as well as the Swedish Research Council VR.

REFERENCES

[1] V. Prakash and R. Mittra, "Characteristic basis function method: A new technique for efficient solution of method of moments matrix equations," *Micr. Opt. Technol.*, vol. 36, pp. 95–100, Jan. 2003.

[2] L. Matekovits, G. Vecchi, M. Bercigli, and M. Bandinelli, "Synthetic-functions analysis of large aperture-coupled antennas," *IEEE Trans. Antennas Propag.*, vol. 57, no. 7, pp. 1936–1943, Jul. 2009.

[3] J. H. Richmond, "On the variational aspects of the moment method," *IEEE Trans. Antennas Propag.*, vol. 39, no. 4, pp. 473–479, Apr. 1991.

[4] R. Maaskant, D. J. Bekers, M. J. Arts, W. A. van Cappellen, and M. V. Ivashina, "Evaluation of the radiation efficiency and the noise temperature of low-loss antennas," *IEEE Antennas Wireless Propag. Lett.*, vol. 8, no. 8, pp. 1536–1225, Jan. 2009.

[5] P. Y.-Oijala and M. Taskinen, "Calculation of cfie impedance matrix elements with RWG and $\boldsymbol{n}\times$RWG functions," *IEEE Trans. Antennas Propag.*, vol. 51, no. 8, pp. 1837–1846, Aug. 2003.

[6] R. Maaskant, "Analysis of large antenna systems," Ph.D. dissertation, Eindhoven University of Technology, Eindhoven, 2010. [Online]. Available: http://alexandria.tue.nl/extra2/201010409.pdf

[7] R. Maaskant, R. Mittra, and A. G. Tijhuis, "Fast analysis of large antenna arrays using the characteristic basis function method and the adaptive cross approximation algorithm," *IEEE Trans. Antennas Propag.*, vol. 56, no. 11, pp. 3440–3451, Nov. 2008.

[8] ——, "Application of trapezoidal-shaped characteristic basis functions to arrays of electrically interconnected antenna elements," in *Proc. Int. Conf. on Electromagn. in Adv. Applicat. (ICEAA)*, Torino, Sep. 2007, pp. 567–571.

[9] L. Matekovits, V. A. Laza, and G. Vecchi, "Analysis of large complex structures with the synthetic-functions approach," *IEEE Trans. Antennas Propag.*, vol. 55, no. 9, pp. 2509–2521, Sep. 2007.